CrossMark

Experimental Research on Static Behavior of Stiffened T-Shaped Concrete-Filled Steel Tubular Stubs Subjected to Concentric Axial Loading

Chuangze Xu[2] · Yuanlong Yang[1,3] · Xin Tang[1,3] · Jiepeng Liu[1,3]

Abstract

Eight stiffened T-shaped concrete-filled steel tubular (CFST) columns and one non-stiffened T-shaped CFST column were tested subjected to axial compressive load in this paper. The mechanical property and failure mode of the specimens were studied. The influences of steel ratio, concrete strength and sectional size were investigated on the axial compressive performance of the specimens. A numerical program was developed to calculate concentric load-shortening curves of T-shaped CFST columns based on experimental results. The confined concrete distribution in T-shaped section and the stiffened tube's local buckling were considered in the numerical program. A good agreement between calculating results and experimental results was obtained. Besides, a design formula of bearing capacity of stiffened T-shaped CFST columns was put forward by considering favorable effect of stiffeners.

Keywords T-shaped column · Concrete-filled steel tubular column · Stiffeners · Local buckling · Failure modes · Bearing capacity

1 Introduction

Rectangular cross-sectional columns in traditional frame structures, with extended corners to indoor space, normally have larger cross-sectional depths than those of adjacent infilled walls, leading to reduction of usable indoor space and disturbance to indoor environment. Recently, special-shaped cross-sectional columns, as an improved architectural approach, have been increasingly introduced into residential and official buildings. Smooth connection between special-shaped columns and adjacent infilled walls guarantees increased efficiency of indoor space and availability to furniture arrangement.

Systematic research and extensive engineering practice have been carried out on reinforced concrete (RC) special-shaped column. Early study mainly focused on the static behavior of T-shaped and L-shaped stub columns subjected to concentric compressive load or biaxial eccentric compressive load, based on which, the interaction curve of *M–N* resistances for practice was proposed (Joaquin 1979; Cheng and Thomas 1989; Mallikarjuna and Mahadevappa 1992, 1994; Dundar and Sahin 1993; Yau et al. 1993). Since 2000, to adapt to development of housing industry, extensive study carried by Chinese researchers has concentrated on comprehensive static and seismic behaviors, especially for RC special-shaped columns in frame structure or frame-shear wall structure (Zhang and Ye 2003; Gao et al. 2005; Wang et al. 2007).

To improve the seismic behavior of special-shaped columns, academic research and engineering promotion of special-shaped concrete-filled steel tubular (CFST) columns have been in the ascendant. Recent research mainly focused on mechanical behavior of stiffened special-shaped CFST columns. The plate rib, which is the most commonly used stiffener in square or circular CFST column, has been introduced into the L-shaped CFST columns (Lin et al. 2009), reinforcing the tube by enlarging bending rigidity of

✉ Yuanlong Yang
yangyuanlong@cqu.edu.cn

1 Key Laboratory of New Technology for Construction of Cities in Mountain Area (Chongqing University), Ministry of Education, Chongqing 400045, China

2 Gansu Province Transportation Planning Survey and Design Institute Co., Ltd., Lanzhou 730000, China

3 School of Civil Engineering, Chongqing University, Chongqing 400045, China

steel plate section. An experiment on this kind of member in frame structures was carried out to investigate its seismic behavior (Zhang et al. 2010). A pulled binding bar was adopted at possible plastic hinge locations in the T-shaped and L-shaped CFST columns subjected to concentric or eccentric load in the experimental and theoretical research (Cai and He 2005; Zuo et al. 2012a, b). A latticed special-shaped column composed of concrete filled steel tubes was experimented subjected to constant axial load and cyclically varying flexural loads (Zhou et al. 2012). This kind of column worked together well and its seismic behavior was good. Based on above research, the special-shaped CFST column is a new type of composite structural member with good prospect, however mechanical efficiency of stiffeners and seismic behavior of special-shaped CFST column are still worth to be improved in the future research.

The authors of this paper have conducted static and seismic experiments of special-shaped CFST columns with tensile bar stiffeners. The tensile bar stiffener has good exploration of steel tension property, low steel amount and convenient fabricating procedure. It can effectively restrain or postpone the local buckling of special-shaped tube and provide sufficient confinement for concrete. Therefore, the increases of bearing capacity, ductility and energy dissipation of special-shaped CFST columns can be expected (Yang et al. 2010, 2012) compared with those of special-shaped RC columns. The design methods have been proposed for special-shaped CFST columns subjected to concentric and eccentric compressive loads (Yang et al. 2015).

An extensive experiment of T-shaped CFST columns with tensile bar stiffener subjected to concentric compressive load is presented in this paper. The parameters of concrete strength, steel yield strength, steel ratio and sectional depth were investigated in this experiment. A theoretical analysis with numerical program was carried out and verified by experimental results. A design formula for predicting resistance, based on experimental and theoretical analysis, was proposed for actual engineering practice.

2 Experimental Study

2.1 Details of Specimens

Nine specimens were designed in this test, including one non-stiffened CFST column TA1 and eight CFST columns with tensile bar stiffeners. The stiffened specimens were divided into four categories: three standard CFST columns (TA2-1, TA2-2 and TA2-3), two columns with smaller sectional depth (TA3-1, TA3-2), one column with higher concrete strength (TA4) and two columns with lower steel yield strength and steel ratio (TA5-1, TA5-2). The specimens were designed with similarity ratio of 1:2.5. The cross-sectional dimensions of stiffened specimens and their constituents are demonstrated in Fig. 1.

The tensile bar stiffeners were welded on the concave corners and on the steel plates with large width-to-thickness ratio (Fig. 1). Holes with diameter slightly larger than those of the stiffeners were reserved in the steel tube for the stiffeners to pass through. The tensile stiffener was then fillet welded with the steel tube at its two ends, with longitudinal spacing of the tensile bar being 100 mm. Therefore, each stiffened cross section is welded with four tensile bars (TA2, TA4 and TA5) or three tensile bars (TA3), and total nine cross sections are stiffened through the height. The parameters of specimens are listed in the Table 1.

Fig. 1 Cross sections of T-shaped CFST columns (unit: mm). **a** Stiffened specimen (TA2, TA4 and TA5) and **b** stiffened specimen with smaller sectional depth (TA3)
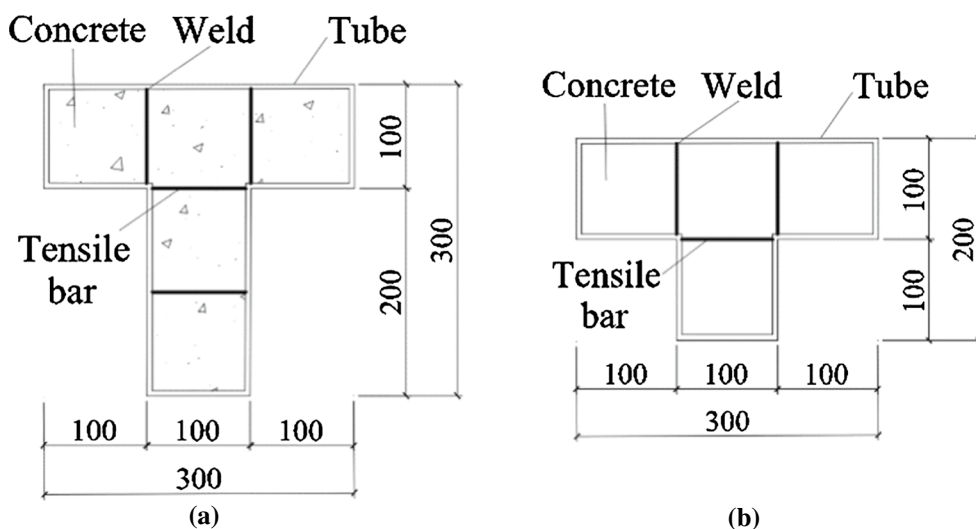
Table 1 Parameters of specimens

| Specimen	Concrete strength f_{ck} (MPa)	Steel tube yielding strength f_y (MPa)	Steel tube thickness t (mm)	Stiffener yielding strength f_s (MPa)	Stiffener diameter d (mm)	Specimen length L (mm)
TA1	36.9	306	3.0	–	–	900
TA2-1	36.9	306	3.0	495	7.0	900
TA2-2	36.9	306	3.0	495	7.0	900
TA2-3	36.9	306	3.0	495	7.0	900
TA3-1	36.9	306	3.0	495	7.0	900
TA3-2	36.9	306	3.0	495	7.0	900
TA4	42.9	306	3.0	495	7.0	900
TA5-1	36.9	232	2.0	495	7.0	900
TA5-2	36.9	232	2.0	495	7.0	900

Fig. 2 Loading device and measuring apparatus. **a** Picture of loading and **b** simple diagram of loading

(a)

(b)
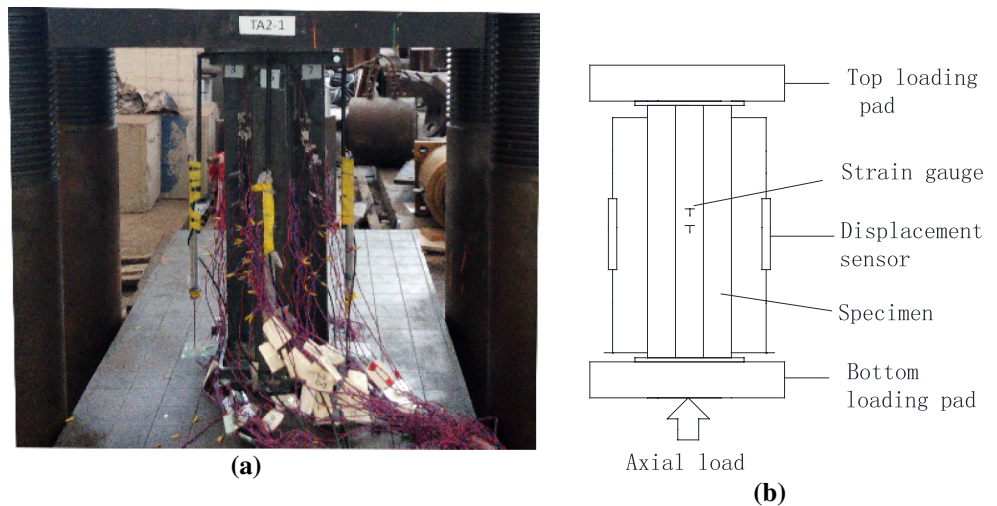
2.2 Experimental Devices and Measuring Apparatus

The experimental was carried out at the structural laboratory of Chongqing University and a 1000-ton pressure press was used as loading device (shown in Fig. 2). The specimen is simulated as fixed boundary condition. A force–displacement hybrid loading scheme was used during the test. 20% of estimated yield load was employed as load increment before yielding. Afterwards, the test continued at a rate of 0.01 mm/s in displacement control. In order to eliminate virtual displacement, 30% of predicted ultimate bearing capacity was applied for preloading before formal loading. Four displacement sensors were used to collect data respectively fixed on four sides of the specimen. Strain gauges were displayed on mid-height steel tube for monitoring strain development and physical centering. Actual load was real-timely monitored on the pressure press and recorded in every loading step. When the load reduced to 85% of the peak load, the specimen was taken as failure and the loading procedure was stopped.

Fig. 3 Numbering of T-shaped tube surfaces
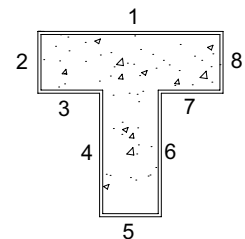
3 Test Phenomenon

To describe experimental phenomenon conveniently, all the steel tube surfaces in cross sections are numbered in Fig. 3.

(a)

(b)

Fig. 4 Failure mode of specimen TA1. **a** Local buckling of steel tube and **b** concrete damage

3.1 Test Phenomenon of Non-stiffened T-Shaped CFST Column (Specimen TA1)

Figure 4 illustrates the ultimate failure mode of specimen TA1 by investigating the local buckling of steel tube and concrete damage emphasized with ellipses in the figures. When loading to 1600 kN, the buckling firstly occurred on the steel plate 1 (Fig. 4a). Before reaching peak load, most local buckling appeared on the steel plate 1 and 6 (Fig. 4a), whose depth-to-thickness ratio are larger than other plates. When reaching the peak load, a loud noise was heard and then the load fell sharply. After the experiment, the largest buckling was detected on the steel plate 6, with buckling height being 15 mm (Fig. 4a). By removing steel tube, crushed concrete was observed with mass concrete split off from web of the specimen and some longitudinal cracks

were observed on most surfaces (Fig. 4b). The above phenomenon revealed that relatively weak confinement provided by non-stiffened steel tube resulted in specimen's brittle failure. The strength and ductility of steel tube and concrete were not utilized sufficiently.

3.2 Test Phenomenon of Standard Stiffened CFST Columns (Specimens TA2)

According to axial load–displacement curves, the local buckling loads of three specimens TA2-1, TA2-2 and TA2-3 were 2200 kN, 1800 kN and 2000 kN respectively. Take the specimen TA2-2 as an example to introduce the test phenomenon after experiment. A multi-wave buckling mode was observed at steel plates 3, 4, 6 of the specimen
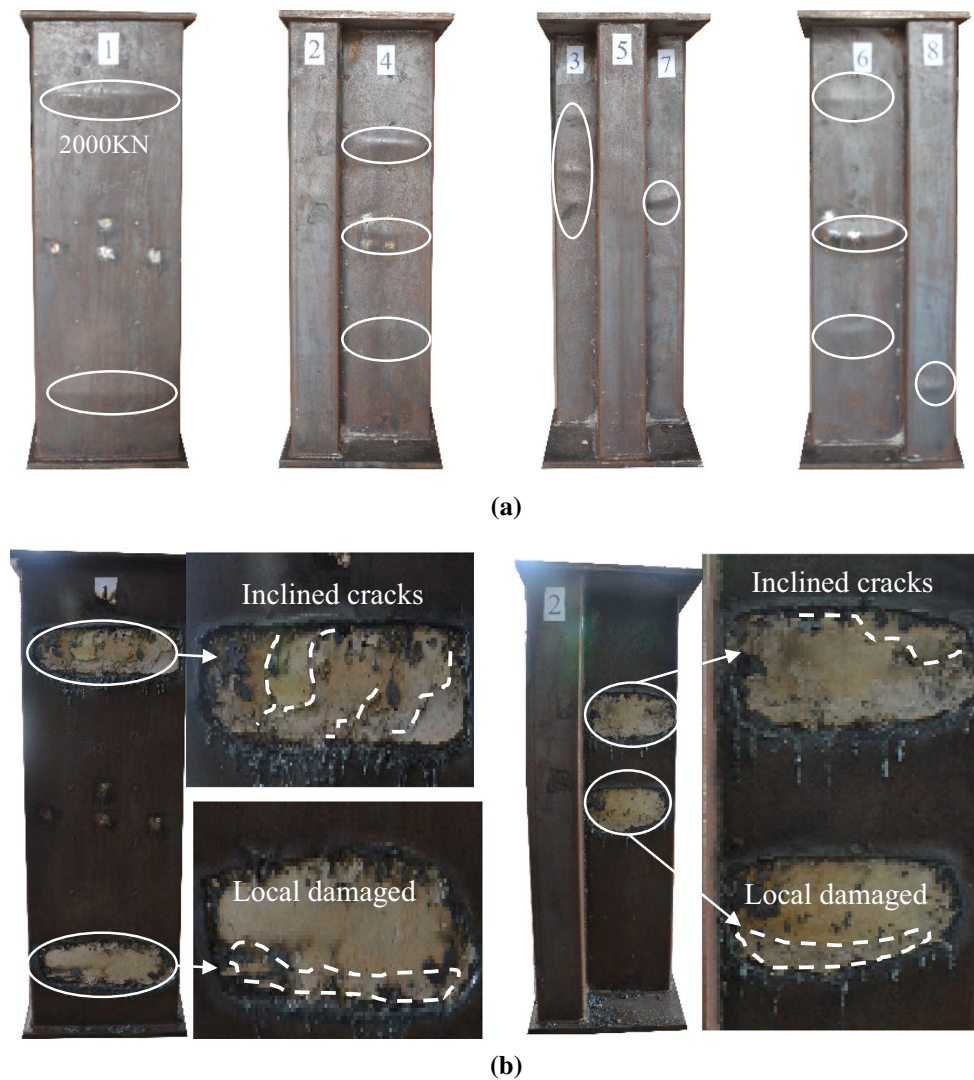
(a)

(b)

Fig. 5 Failure mode of specimens TA2. **a** Local buckling of steel tube and **b** concrete damage

(Fig. 5a). The largest buckling appeared at the web area of surface 6, with the buckling height being 12 mm (Fig. 5a). The tensile bars effectively restrained the buckling of its neighboring steel tube, thus all the buckles were observed on the non-stiffened steel plate between adjacent stiffeners. By tapping the buckles, no separation was detected between concrete and steel tube. After removing the buckling steel plates, local damaged concrete and some inclined cracks were observed (Fig. 5b). The deformation at concave corners was nearly completely restrained by bar stiffeners. Above all, compared with the non-stiffened specimen TA1, the bar stiffener postponed the local buckling of steel tube, increased the buckling bearing capacity, improved the confinement for concrete and transmitted the failure mode of concrete from brittle splitting damage to local crushed damage.

3.3 Test Phenomenon of Specimens TA3, TA4 and TA5

The test phenomenon of specimens TA3, TA4 and TA5 are similar with those of specimens TA2. The specimen TA3 has small sectional depth. The local buckles were mainly detected on the steel plate 1 with large depth-to-thickness ratio. The specimen TA4, with higher concrete strength, possessed larger yield resistance and peak resistance than standard specimen TA2. The thin-walled specimens TA5 had serious local buckles observed on all the tube surfaces. Multi-wave buckling mode was detected on the tube surfaces with large depth-to-thickness ratio.

Fig. 6 Axial concentric load–displacement curves

(a)

(b)

(c)

(d)
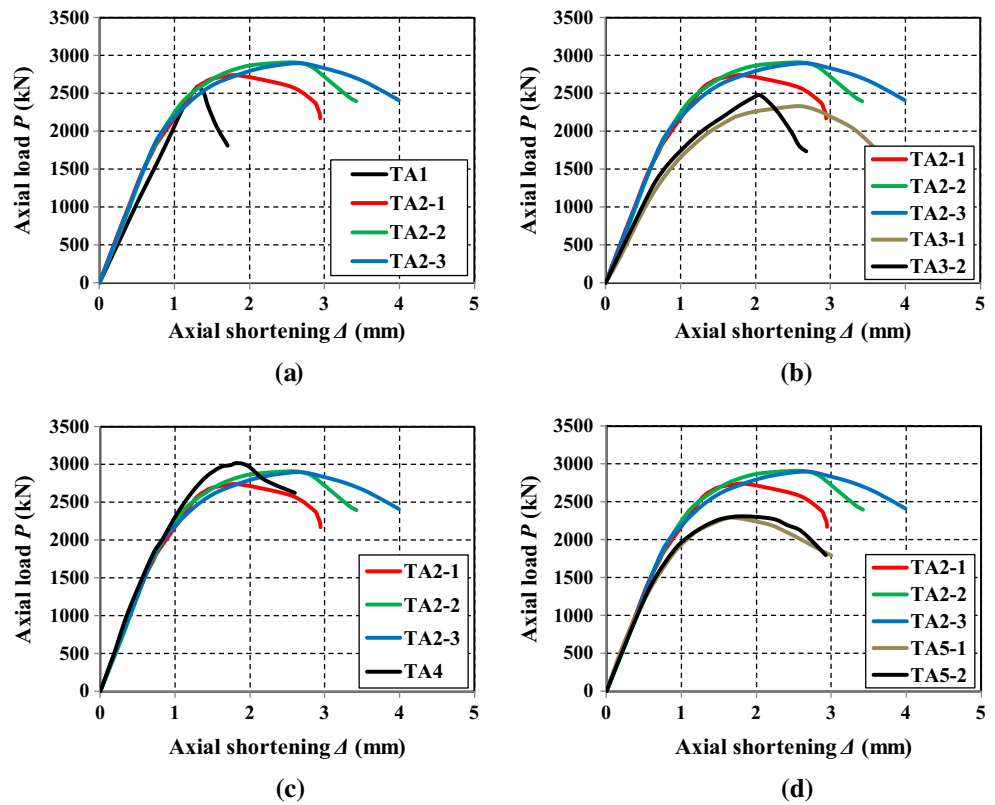
4 Axial Concentric Load–Displacement Curves and Mechanical Performance Index

The axial load was measured with a load sensor in the 1000-ton pressure press and four displacement sensors (LVDT) connected to strain acquisition system were used for measuring axial displacement. Axial concentric load–displacement curves were shown in several groups in the Fig. 6 divided according to analytical investigative parameters. The mechanical performance index based on the test curves were listed in Table 2.

Compared to the specimen TA1, the bearing capacity and ductility were both obviously increased by setting stiffeners in the specimens TA2 (shown in Fig. 6a). The peak bearing capacity was increased by 6–12% and the ductility coefficient was increased by 125–325%. The main reason is that the bar stiffener can effectively postpone the local buckling of steel tubes. At the same time, the separation

Table 2 Mechanical performance indexes

Specimen	Buckling bearing capacity P_b (kN)	Experimental bearing capacity P_e (kN)	Ductility coefficient μ	Ductility enhancement coefficient E_μ
TA1	1600	2589	1.2	1.00
TA2-1	2200	2743	3.6	3.0
TA2-2	1800	2908	4.2	3.5
TA2-3	2000	2897	4.6	3.8
TA3-1	2000	2332	5.1	4.3
TA3-2	1600	2472	3.6	3.0
TA4	2400	3020	2.7	2.3
TA5-1	1000	2288	4.3	3.6
TA5-2	800	2331	4.2	3.5

Ductility coefficient is the ratio of ultimate displacement (corresponding to 85% of peak bearing capacity) to yield displacement. The yield displacement is determined with yield strain of steel tube or stiffness reduction of load–displacement curve

between concrete and tube was significantly reduced and the confinement provided for concrete by stiffened tube was relatively increased.

Comparing the specimens TA2 and TA3 in Fig. 6b, the former one took advantage on the later one in bearing capacity, ductility and rigidity, illustrating that sectional depth had obviously effected on mechanical properties. The ratio of test bearing capacity to superposed bearing capacity of specimens TA2 and TA3 were similar, which showed that the mechanical properties are improved only because of the increase of material amount.

Compared to the specimens TA2, the ultimate bearing capacity of specimen TA4 with higher concrete strength was increased by 4–10%. While the ductility of specimen is slightly reduced, because brittle failure of concrete is more obvious when increasing the concrete strength (shown in Fig. 6c).

The bearing capacity and stiffness of specimens TA5 were both worse than specimens TA2 (shown in Fig. 6c), owing to low steel yield strength and low steel ratio. Although the confinement for concrete is larger when the steel tube is thicker, the buckling of thicker tube will bring more reduction of bearing capacity and confinement. Therefore, the ductility of specimens TA2 was not improved compared with specimens TA5.

5 Numerical Analysis

Axial load-shortening relationship curves of specimens are calculated by a numerical program with Fortran software developed in this paper. The uniaxial nonlinear stress–strain relationships were used as constitutive models of concrete and steel in the program. The confined concrete distribution and local buckling of stiffened steel plates are considered in the program.

5.1 Uniaxial Stress–Strain Relationship of Confined Concrete

The mechanical behavior and deformation of T-shaped CFST columns are more complicated than square or circle columns. Referred to author's previous research (Yang et al. 2015), the confined concrete distribution of non-stiffened T-shaped CFST section is proposed in Fig. 7a.

The tensile bar stiffened CFST column has two typical cross sections: stiffened section (stiffeners are located here) and non-stiffened section (the middle section between two stiffened sections). The tensile bar, which are welded at the steel plates with large depth-to-thickness ratio and at the concave corners, converts previous non-confined region into confined region at welds. Accordingly, sectional confined region increases to larger region in Fig. 7b. The points A and B are in the stiffened section and the points C and D are in the non-stiffened section. The cross-sectional boundary line of confined concrete and non-confined concrete is estimated with second-order parabola.

The Fig. 8 shows the longitudinal distribution of confined concrete. The stiffened section 1-1 has the largest confined concrete region. The non-stiffened section 2-2, with the
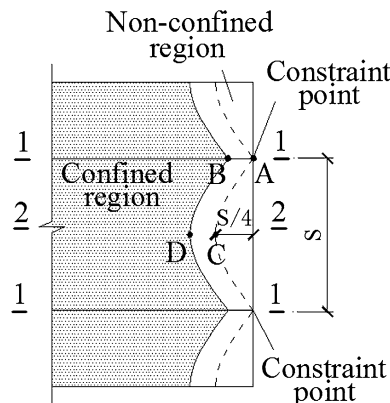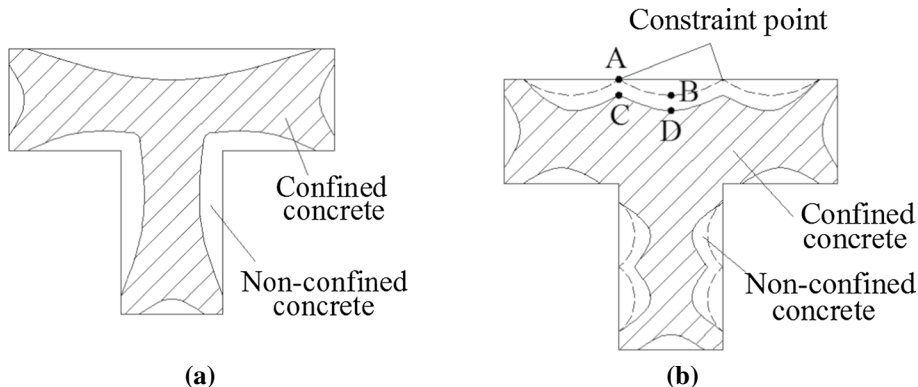
Fig. 8 Vertical constraint concrete region

Fig. 7 Cross-sectional constraint concrete region of T-shaped CFST. **a** Confined concrete distribution in non-stiffened CFST section and **b** confined concrete distribution in stiffened CFST section

(a)

(b)

smallest confined concrete region, is the most likely damaged section, thus it directly determines member's mechanical behavior. The resistance of section 2-2 can be considered as the resistance of the tensile bar stiffened CFST column. The longitudinal boundary line of confined concrete and non-confined concrete is estimated with second-order parabola between two adjacent stiffened sections. Compared with Figs. 7b and 8, point C is corresponding point in the non-stiffened section which point A extends along longitudinal boundary line; point D is corresponding point in the non-stiffened section which point B extends along longitudinal boundary line. The detailed dimensions of confined concrete region can refer to author's previous research (Yang et al. 2015).

The tensile bars transform the T-shaped CFST column into several equivalent rectangular CFST parts (Fig. 9). The distribution of confined concrete of every part is similar with rectangular CFST column. The lateral pressure f_{li} at concrete outer boundary by steel tube in rectangular CFST column is calculated as

$$f_{li} = 0.2 f_y t / L_i \tag{1}$$

where the L_i is cross-sectional dimension of concrete; the t is thickness of steel plate.

Weight the lateral pressure f_{li} to obtain the average lateral pressure f_i: at concrete outer boundaries:

$$f_l = \sum_{i=1}^{m} f_{li} L_i \bigg/ \sum_{i=1}^{m} L_i \tag{2}$$

where m is number of steel plates in rectangular tubes transformed from T-shaped tube.

The confinement effective coefficient k_e is defined as ratio of the area of confined concrete A_{cc} to the area of all the concrete A_c:

$$K_e = \frac{A_{cc}}{A_c} \tag{3}$$

The uniformly distributed lateral pressure f_l' in the whole concrete section is defined as

$$f_l' = k_e f_l \tag{4}$$

Then regress the compressive strength of confined concrete f_{cc} by Mander's concrete model (Mander et al. 1988):

$$f_{cc} = f_{ck}(-7.333(f_l'/f_{ck})^2 + 6.533(f_l'/f_{ck}) + 1) \tag{5}$$

The peak strain of confined concrete ε_{cc} is calculated by the following formula with the compressive strength of confined concrete f_{cc}

$$\varepsilon_{cc} = \varepsilon_{ck}\left[1 + 5\left(\frac{f_{cc}}{f_{ck}} - 1\right)\right] \tag{6}$$

Confined concrete and non-confined concrete separately employ their stress–strain curves. The stress–strain curve of non-confined concrete employs the appendix C in the Code for design of concrete structures (GB50010-2010) and the stress–strain curve of confined concrete employs the concrete model in this paper.

5.2 Uniaxial Stress–Strain Relationship of Steel Tube

For steel plates, when depth-to-thickness ratio B/t is larger than $60\sqrt{235/f_y}$, local buckling and its effect on bearing capacity should not be ignored, so the elastic buckling strength of stiffened steel plates is proposed

$$f_{cr}' = \alpha_a \alpha_b f_{cr} = \alpha_a \alpha_b \frac{\pi^2 D}{b^2}\left(4\varphi^2 + \frac{4}{\varphi^2} + \frac{8}{3}\right) \tag{7}$$

where α_a and α_b are longitudinal and transversal spacings of stiffeners.

For the steel plates with depth-to-thickness ratio less than $60\sqrt{235/f_y}$, local buckling can be ignored and the buckling strength of steel tube f_{cr}' equals to yield strength

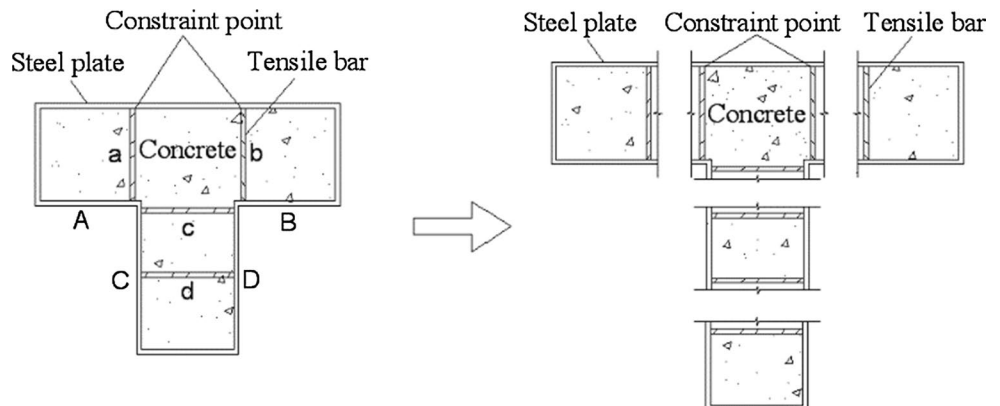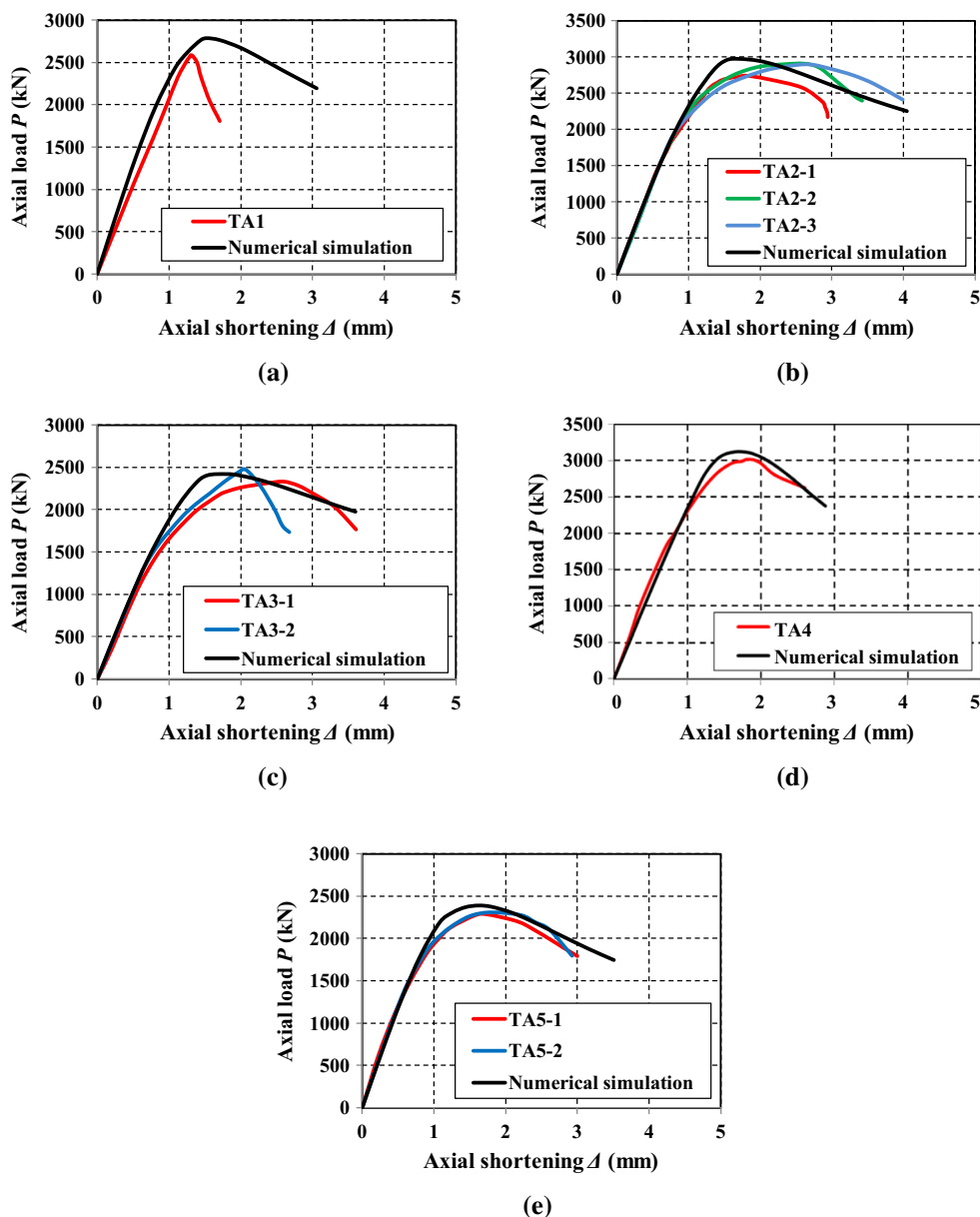**Fig. 9** Cross-sectional simplification of T-shaped CFST

Fig. 10 Comparison of experimental and theoretical curves

(a)

(b)

(c)

(d)

(e)

f_y. The details of uniaxial stress–strain relationship of steel tube can refer to document (Mander et al. 1988).

The bearing capacities of concrete and steel tube are then superimposed to obtain the bearing capacity of specimen as follows

$$N = N_c + N_s = f_{cc}A_c + f'_{cr}A_s \qquad (8)$$

The concentrically compressive load-shortening curves of stiffened T-shaped CFST columns agree well with the test curves (Fig. 10). The numerical model proposed in this paper can be used for predicting the mechanical behavior of stiffened T-shaped CFST columns.

6 Comparison of the Test Bearing Capacity, Superposed Value and Design Values of European, American and Chinese Codes

The mainstream design Codes of square and rectangular CFST columns are ANSI/AISC 360-10, EC4 (2004) and GB 50936-2014. The stiffened T-shaped concrete-filled steel tubular stubs can be approximately calculated with these codes.

6.1 Design Bearing Capacity in ANSI/AISC 360-10

The bearing capacity N_u is calculated with the following formulas:

$$N_u = P_0 \left[0.658^{\frac{P_0}{P_e}} \right] \quad \text{when } P_e \geq 0.44 P_0 \tag{9a}$$

$$N_u = 0.877 P_e \quad \text{when } P_e < 0.44 P_0 \tag{9b}$$

$$P_0 = f_y \cdot A_s + 0.85 f_{ck} \cdot A_c \tag{10}$$

$$P_e = \frac{\pi^2 (EI)_{eff}}{L^2} \tag{11}$$

$$(EI)_{eff} = E_s I_s + c \cdot E_c I_c \tag{12}$$

$$c = 0.6 + 2 \left(\frac{A_s}{A_c + A_s} \right) \tag{13}$$

in which the P_0 is nominal compressive bearing capacity of composite member; the P_e is elastic critical buckling bearing capacity; the $(EI)_{eff}$ is effective bending stiffness of composite section; the E_s and E_c are elastic modulus of steel and concrete; the I_s and I_c are moment of inertia of steel section and the concrete section about the elastic neutral axis; the A_s and A_c are areas of the steel and concrete; the c is coefficient for calculation of effective bending stiffness.

6.2 Design Bearing Capacity in EC4 (2004)

The bearing capacity N_u is calculated with the following formulas:

$$N_u = \varphi N_{pl,rd} \tag{14}$$

$$\varphi = \frac{1}{\phi + \sqrt{\phi^2 - \bar{\lambda}^2}} \leq 1.0 \tag{15}$$

$$\phi = 0.5 \left[1 + 0.34 \left(\bar{\lambda}^2 - 0.2 \right) + \bar{\lambda}^2 \right] \tag{16}$$

$$N_{pl,rd} = f_y \cdot A_s + f_{ck} \cdot A_c \tag{17}$$

$$\bar{\lambda} = \sqrt{\frac{N_{pl,rd}}{N_{cr}}} \tag{18}$$

$$N_{cr} = \frac{\pi^2 (EI)_{eff}}{L^2} \tag{19}$$

$$(EI)_{eff} = E_s I_s + 0.6 E_c I_c \tag{20}$$

in which the $N_{pl,rd}$ is plastic resistance to compression; the φ is reduction factor for the relevant buckling mode; the φ is value to determine the reduction factor φ; the $\bar{\lambda}$ is relative slenderness; the N_{cr} is elastic critical normal force.

6.3 Design Bearing Capacity in GB 50936-2014

The design bearing capacity in GB 50936-2014 is proposed based on the unified theory. In the unified theory, the CFST column is treated as a unified compound material without distinguishing steel tube and concrete. Performance indexes of the compound material is obtained by testing regression. The bearing capacity of column is calculated by its whole geometry features and composite performance indexes of CFST.

The bearing capacity N_u is calculated with the following formulas:

$$N_u = \varphi N_0 \tag{21}$$

$$\varphi = \frac{1}{2\bar{\lambda}_{sc}^2} \left[\bar{\lambda}_{sc}^2 + \left(1 + 0.25 \bar{\lambda}_{sc} \right) - \sqrt{\left(\bar{\lambda}_{sc}^2 + \left(1 + 0.25 \bar{\lambda}_{sc} \right) \right)^2 - 4 \bar{\lambda}_{sc}^2} \right] \tag{22}$$

$$\bar{\lambda}_{sc} = \frac{\lambda_{sc}}{\pi} \sqrt{\frac{f_{sc}}{E_{sc}}} \approx 0.01 \lambda_{sc} \left(0.001 f_y + 0.781 \right) \tag{23}$$

$$N_0 = A_{sc} \cdot f_{sc} \tag{24}$$

$$A_{sc} = A_c + A_s \tag{25}$$

$$f_{sc} = \left(1.212 + B \cdot k \cdot \theta_{sc} + C \cdot k^2 \cdot \theta_{sc}^2 \right) f_{ck} \tag{26}$$

$$\theta_{sc} = \alpha_{sc} \frac{f_y}{f_{ck}} \tag{27}$$

$$\alpha_{sc} = \frac{A_s}{A_c} \tag{28}$$

$$B = 1.131 \frac{f_y}{235} + 0.723 \tag{29}$$

$$C = -0.07 \frac{f_{ck}}{20.1} + 0.0262 \tag{30}$$

$$k = 1.0 \tag{31}$$

in which the N_0 is composite bearing capacity of CFST; the φ is stability factor of CFST; the $\bar{\lambda}_{sc}$ is non-dimensional slenderness ratio; the λ_{sc} is slenderness ratio; the E_{sc} is composite bending modulus; the A_{sc} is area of CFST section; the f_{sc} is composite strength of CFST; the θ is confining coefficient;

Table 3 The comparison of bearing capacities

Specimens	Test P_e (kN)	Simply superposition P_n (kN)	EC4 P_E (kN)	AISC P_A (kN)	GB 50936-2014 P_C (kN)	Prediction P_P(kN)
		($E_1 = P_e/P_n$)	($E_2 = P_e/P_E$)	($E_3 = P_e/P_A$)	($E_4 = P_e/P_C$)	($E_5 = P_e/P_P /$)
TA1	2589	2812 (0.92)	2812 (0.92)	2538 (1.02)	3098 (0.84)	2787 (0.93)
TA2-1	2743	2812 (0.98)	2812 (0.97)	2538 (1.08)	3098 (0.89)	2973 (0.92)
TA2-2	2908	2812 (1.03)	2812 (1.03)	2538 (1.15)	3098 (0.94)	2973 (0.98)
TA2-3	2897	2812 (1.03)	2812 (1.03)	2538 (1.14)	3098 (0.94)	2973 (0.97)
TA3-1	2332	2282 (1.02)	2282 (1.02)	2065 (1.13)	2498 (0.93)	2421 (0.96)
TA3-2	2472	2282 (1.08)	2282 (1.08)	2065 (1.20)	2498 (0.99)	2421 (1.02)
TA4	3020	3093 (0.98)	3093 (0.96)	2771 (1.09)	3445 (0.88)	3117 (0.97)
TA5-1	2288	2303 (0.99)	2303 (0.99)	2275 (1.01)	2855 (0.80)	2389 (0.96)
TA5-2	2331	2303 (1.01)	2303 (1.01)	2275 (1.02)	2855 (0.82)	2389 (0.98)
TA2[1]	2672	2476 (1.08)	2476 (1.08)	2288 (1.17)	2612 (1.02)	2562 (1.04)
TA3[1]	2259	1917 (1.18)	1917 (1.18)	1696 (1.33)	2055 (1.10)	2157 (1.05)
TA4[1]	2549	2476 (1.03)	2476 (1.03)	2288 (1.11)	2612 (0.98)	2767 (0.92)
TA5[1]	2827	2476 (1.14)	2476 (1.14)	2288 (1.24)	2612 (1.08)	2767 (1.02)

Simply superposition of bearing capacity $P_n = f_y \cdot A_s + f_c \cdot A_c$

The specimens TA2[1], TA3[1], TA4[1], TA5[1] are the test data in document (Yang et al. 2015). The TA2[1] is non-stiffened CFST column; the TA3[1] and TA4[1] are CFST columns with battlement-shaped bar stiffener; the TA5[1] is CFST column with tensile bar stiffener

P_P is calculated bearing capacity of the numerical program in this paper

the α_{sc} is steel ratio; the B and C are influence coefficients of section on constraint effect.

The comparison in bearing capacity of the simply superposition, the calculation value in above codes and the test value is listed in the Table 3.

The average ratio of test value to EC4 value ($E_2 = P_e/P_E$) is 1.03; the average ratio of test value to AISC value ($E_3 = P_e/P_A$) is 1.13. The design values of AISC and EC4 are a little conservative compared to test values. The average ratio of test value to GB 50936-2014 value ($E_4 = P_e/P_C$) is 0.94. The average ratio of test value to numerical program value ($E_5 = P_e/P_P$) is 0.98. The tensile bar stiffeners in T-shaped CFST column can only increase the confinement to a limited extent. The confinement in T-shaped CFST column is still smaller than that in square CFST column.

Considering the confinement for concrete and the improvement of the steel tube buckling by stiffeners, the design bearing capacity N of stiffened T-shaped CFST short column is proposed based on the superposition formula by introducing modified coefficient $\overline{E_1}$:

$$N = \overline{E_1}\left(f_y \cdot A_s + f_c \cdot A_c\right) \tag{32}$$

where $\overline{E_1}$ is the average ratio of test value of specimens with stiffeners P_e to simply superposition value P_n, suggested as 1.04 according to Table 3. It should be noted that more experiment with large parameter range should be further conducted to collected data to verify this value.

7 Conclusions

1. For the T-shaped short CFST columns, concrete and steel tube worked together. The tensile bar stiffeners can effectively restrain the outward deformation of concave corners and weld points, postpone the local buckling of steel tubes, improve the confinement of concrete in a

certain extent, increase the bearing capacity and ductility of specimens and improve the failure mode of specimens.

2. The bearing capacity of specimens can be effectively improved when increasing the steel ratio, concrete strength and sectional size.

3. The axial load-shortening relationship curves were calculated with a numerical program with FORTRAN software which considering the concrete confinement stiffening mechanism of steel tube in this paper. The numerical program can be used to predict the bearing capacity of stiffened T-shaped CFST short column within the allowable error range.

4. The design formula of bearing capacity of stiffened T-shaped CFST columns is proposed in this paper. The concrete confinement and stiffening mechanism of steel tube are considered in the formula, which is reasonably accurate based on test.

References

Cai, J., & He, Z. Q. (2005). Axial load behavior of square CFT stub column with binding bars. *Journal of Constructional Steel Research, 62,* 472–483.

Cheng, T., & Thomas, H. (1989). T-shaped reinforced concrete members under biaxial bending and axial compression. *ACI Structural Journal, 86*(4), 2576–2595.

Dundar, C., & Sahin, B. (1993). Arbitrarily shaped reinforced concrete members subjected to biaxial bending and axial load. *Computers & Structures, 49*(4), 643–662.

Gao, D. X., Ke, J., & Wang, L. H. (2005). Seismic behavior analysis of special-shaped column frame structure. *Journal of Xi'an University of Technology, 21*(3), 285–288. **(in Chinese)**.

Joaquin, M. (1979). Design aids for L-shaped reinforced concrete columns. *ACI Structural Journal, 76*(49), 1197–1216.

Lin, Z. Y., Shen, Z. Y., & Luo, J. H. (2009). Hysteretic behavior of concrete-filled L-section steel tubular columns under cyclic loading. *Progress in Steel Building Structures, 11*(2), 12–17. **(in Chinese)**.

Mahadevappa, P., & Mallikarjuna, (1994). Computer-aided analysis of reinforced concrete columns subjected to axial compression and bending. Part II: T-shaped sections. *Computers & Structures, 53*(6), 1317–1356.

Mallikarjuna, & Mahadevappa, P. (1992). Computer aided analysis of reinforced concrete columns subjected to axial compression and bending: I. L-shaped sections. *Computers & Structures, 44*(5), 1121–1138.

Mander, J. B., Priestley, M. J. N., & Park, R. (1988). Theoretical stress-strain model for confined concrete. *Journal of Structural Engineering, 114*(8), 1804–1826.

Wang, T. C., Li, X. H., Wang, T. Z., et al. (2007). Hysteretic behavior of frame with specially shaped columns subjected to cyclic loading. *Journal of Jilin University (Engineering and Technology Edition), 37*(1), 224–228. **(in Chinese)**.

Yang, Y. L., Wang, Y. Y., & Fu, F. (2015). Static behavior of T-shaped concrete-filled steel tubular columns subjected to concentric and eccentric compressive loads. *Thin-Walled Structures, 95,* 374–388.

Yang, Y. L., Wang, Y. Y., & Zhang, S. M. (2012). Experimental research on seismic behavior of T-shaped concrete-filled steel tube columns with reinforcement stiffeners. *Journal of Building Structures, 33*(4), 104–112. **(in Chinese)**.

Yang, Y. L., Yang, H., & Zhang, S. M. (2010). Compressive behavior of T-shaped concrete filled steel tubular columns. *International Journal of Steel Structures, 10*(4), 419–430.

Yau, C. Y., Chan, S. L., & So, A. K. W. (1993). Biaxial bending design of arbitrarily shaped reinforced concrete column. *ACI Structural Journal, 90*(3), 269–279.

Zhang, J. C., Shen, Z. Y., Lin, Z. Y., et al. (2010). Experimental research on seismic behavior of concrete-filled L-shaped steel tubular frames. *Journal of Building Structures, 31*(8), 1–7. **(in Chinese)**.

Zhang, D., & Ye, X. G. (2003). Non-linear analysis of special-shaped reinforced concrete columns. *Journal of Hefei University of Technology, 26*(4), 490–494. **(in Chinese)**.

Zhou, T., Chen, Z. H., & Liu, H. B. (2012). Seismic behavior of special shaped column composed of concrete filled steel tubes. *Journal of Constructional Steel Research, 75,* 131–141.

Zuo, Z. L., Cai, J., Yang, C., et al. (2012a). Axial load behavior of L-shaped CFT stub columns with binding bars. *Engineering Structures, 37,* 88–98.

Zuo, Z. L., Cai, J., Yang, C., et al. (2012b). Eccentric load behavior of L-shaped CFT stub columns with binding bars. *Journal of Constructional Steel Research, 72,* 105–118.